Selectivity of Electronic Coherence and Attosecond Ionization Delays in Strong-Field Double Ionization

Yuki Kobayashi,[1,*] Maurizio Reduzzi,[1] Kristina F. Chang,[1] Henry Timmers,[1]
Daniel M. Neumark,[1,2,†] and Stephen R. Leone[1,2,3,‡]

[1]*Department of Chemistry, University of California, Berkeley, California 94720, USA*
[2]*Chemical Sciences Division, Lawrence Berkeley National Laboratory, Berkeley, California 94720, USA*
[3]*Department of Physics, University of California, Berkeley, California 94720, USA*

Experiments are presented on real-time probing of coherent electron dynamics in xenon initiated by strong-field double ionization. Attosecond transient absorption measurements allow for characterization of electronic coherences as well as relative ionization timings in multiple electronic states of Xe^+ and Xe^{2+}. A high degree of coherence $g = 0.4$ is observed between $^3P_2^0$-$^3P_0^0$ of Xe^{2+}, whereas for other possible pairs of states the coherences are below the detection limits of the experiments. A comparison of the experimental results with numerical simulations based on an uncorrelated electron-emission model shows that the coherences produced by strong-field double ionization are more selective than predicted. Surprisingly short ionization time delays, 0.85 fs, 0.64 fs, and 0.75 fs relative to Xe^+ formation, are also measured for the $^3P_2$, $^3P_0$, and $^3P_1$ states of Xe^{2+}, respectively. Both the unpredicted selectivity in the formation of coherence and the subfemtosecond time delays of specific states provide new insight into correlated electron dynamics in strong-field double ionization.

Electronic coherence in matter drives electronic motion that is faster than nuclear motion. Recent developments in attosecond light sources produced by high-harmonic generation have enabled the measurements of electronic motion at its natural timescale [1–3]. The past decade has witnessed a great success in the reconstruction of electronic wave packets in atomic and molecular systems [4–10]. One of the current frontiers in the investigation of electronic coherence is to unravel the coherence preparation mechanisms and ultimately to manipulate the electron dynamics and the subsequent nuclear dynamics [11].

Pioneering experimental work using attosecond transient absorption spectroscopy has demonstrated that strong-field ionization (SFI) driven by few-cycle laser pulses is capable of launching coherent electronic wave packets in atomic valence orbitals [4,5]. Among various optical excitation processes, SFI is of particular importance, as it is the first step in all strong-field phenomena such as above-threshold ionization and high-harmonic generation [12]. The coherence preparation mechanisms of SFI have been modeled using the static ionization rate by Ammosov-Delone-Krainov (ADK) theory [13], and results comparable to those of full quantum calculations have been obtained [14–16]. On the other hand, an exact description of SFI requires inclusion of electron correlation, a fundamental many-body effect that is not captured within the single-active electron approximation. The term *electron correlation* is used in ionization dynamics to refer to an adaptation of bound electrons to a change in the binding fields after ionization;

shakeup and shakeoff, for example, are well known as prominent effects [17–19]. The effect of electron correlation in SFI is manifested in ionization timings as demonstrated by attoclock experiments on sequential double ionization, which results in earlier emission of second electrons than predicted by an uncorrelated electron-emission model [20,21]. Although hints of electronic coherence produced by strong-field multiple ionization have been reported [22], the effects of electron correlation on the formation of electronic coherence remain an open question.

In this Letter, we perform attosecond transient absorption spectroscopy on xenon in the multiple-ionization field-intensity regime where the effect of electron recollision-induced double ionization should be limited. The all-optical transient absorption measurements provide quantitative evaluation of electronic coherences formed in Xe^+ and Xe^{2+}, as well as state-resolved information about ionization time delays in strong-field double ionization. The conventional term symbols $^{2S+1}L_J^m$ are used to represent atomic energy states [23]. Between the states $^3P_2^0$-$^3P_0^0$ of Xe^{2+}, a high degree of coherence $g = 0.4$ is observed, whereas for two other possible pairs of states, $^3P_2^1$-$^3P_1^1$ of Xe^{2+} and $^2P_{3/2}^{1/2}$-$^2P_{1/2}^{1/2}$ of Xe^+, the coherences are found to be below the detection limits of the experiments, $g < 0.09$ and $g < 0.02$, respectively. The ionization delays with respect to the Xe^+ signal measured for the $^3P_2$, $^3P_0$, and $^3P_1$ states of Xe^{2+} are 0.85 fs, 0.64 fs, and 0.75 fs, respectively. The coherence and ionization time delays in

the experiments are compared with numerical simulations based on an uncorrelated electron-emission model developed previously for sequential double ionization [14]. Neither the selectivity in coherence nor the subfemtosecond time delays of specific states are predicted in the model, a result suggestive of the role of electron correlation in strong-field double ionization.

A schematic of the experimental setup is shown in Fig. 1(a). The near-infrared (NIR) output of a carrier-envelope phase stable Ti:sapphire laser system (800 nm, 1.8 mJ, 1 kHz) is focused into a neon-filled stretched hollow-core fiber. The spectrally broadened output (750 nm, 0.9 mJ, $\Delta\lambda > 300$ nm) is compressed temporally by compensating the dispersion with chirped mirrors and an ammonium dihydrogen phosphate plate [24]. A near-Fourier-transform-limit 3.5-fs pulse is characterized by a d-scan measurement [25], and the peak field intensity estimated from the beam focus diameter ($\phi_{NIR} \sim 80~\mu m$) is
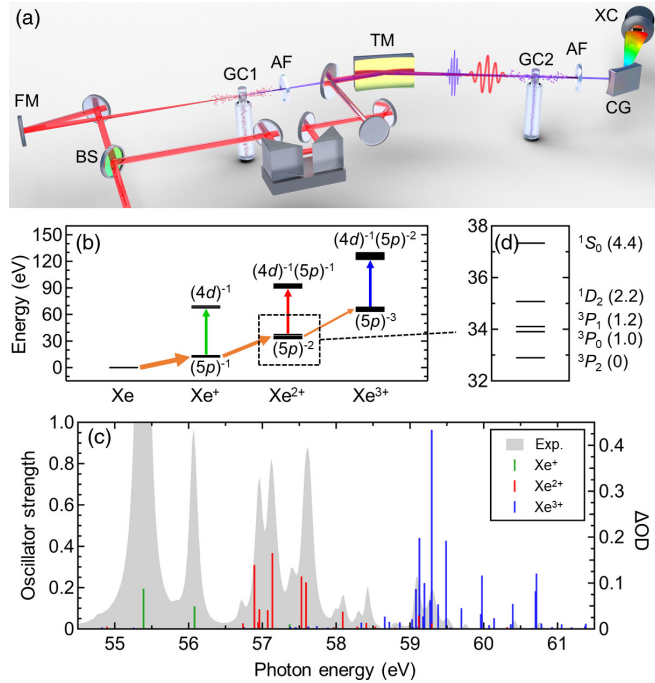

FIG. 1. (a) Schematic of the experimental setup. The red beam represents few-cycle NIR pulses, and the blue beam represents attosecond XUV pulses. AF, aluminum filter; BS, beam splitter; CG, concave grating; FM, focusing mirror; GC1, gas cell for high-harmonic generation; GC2, gas cell for absorption measurements; TM, toroidal mirror; XC, x-ray camera. (b) Energy-level diagram of Xe^{n+} ($n = 0, 1, 2, 3$). The $5p$ electrons of xenon atoms are ionized by the strong NIR pulses (orange arrows), and the subsequent attosecond XUV pulses excite the $4d$ electrons to the $5p$ holes (vertical arrows). (c) Experimental transient absorption spectrum (gray area, right axis) and calculated oscillator strengths for the $4d$-$5p$ transitions of Xe^{n+} ($n = 1$, 2, 3) (green, red, blue lines, left axis). (d) Fine energy structure of the $(5p)^{-2}$ electronic configuration. The numbers in brackets denote relative energy from the lowest $^3P_2$ state in units of eV.

7×10^{14} W/cm². Part of the beam is used to produce isolated attosecond extreme ultraviolet (XUV) pulses by high-harmonic generation in argon gas. The center photon energy of the XUV spectrum is 60 eV, and isolated attosecond pulses with a duration of 170 as have been previously characterized for similar spectra using streaking measurements [24]. The NIR and XUV pulses, linearly polarized along the same direction, are focused by a gold-coated toroidal mirror into an absorption gas cell filled with xenon gas at 6 Torr [26]. The beam focus diameter of the XUV pulse is $\phi_{XUV} \sim 20~\mu m$. The transmitted XUV spectrum is measured by an x-ray spectrometer that consists of an aberration-corrected concave grating (Hitachi 010-0640) and an x-ray-sensitive CCD camera. The improved spectral resolution (< 30 meV) of the spectrometer from our earlier work [29–31] enables us to resolve congested absorption signals from multiple ionic states. The electron dynamics triggered by the NIR pump pulse are monitored by measuring the optical density difference ΔOD defined as the natural logarithm of the ratio between the spectra when the NIR pump is on and off. Active-delay stabilization is implemented to ensure long-term stability of the interferometer [32] and a delay jitter of $\sim$50 as is achieved throughout the measurements.

The energy-level diagram of xenon is shown in Fig. 1(b). The electronic structure is computed using the Cowan suite of atomic structure codes [33]. In the experiments performed, few-cycle strong-field NIR pulses ionize electrons from the $5p$ valence shell (orange arrows), and the subsequent attosecond XUV pulses probe the valence dynamics by $4d$-$5p$ core-to-valence excitation (vertical arrows). Figure 1(c) shows a static transient absorption spectrum plotted together with the calculated $4d$-$5p$ oscillator strengths. At the specified laser-field intensity, singly-, doubly-, and triply-charged ions are produced and characterized.

Electronic coherence is probed by promoting coherent population in the valence states to a common final state, which induces delay-dependent interference modulation in the absorption spectrum [4]. The depth of the modulation is associated with the degree of coherence g, whose definition is given as $g = |\rho_{ij}|/\sqrt{\rho_{ii}\rho_{jj}}$, where ρ is the density matrix and the subscripts i and j are labels of the states. Perfect coherence corresponds to $g = 1$, and complete incoherence yields $g = 0$.

Figure 2(a) shows delay-dependent transient absorption spectra sampled from -5.0 fs to 70.6 fs at a step size of 400 as. A positive delay corresponds to the NIR pulse arriving prior to the XUV pulse, and vice versa for the negative delay. Delay-dependent quantum beats are clearly visible for several transient absorption peaks over the entire positive-delay range. Quantitative analysis is performed by taking a Fourier transformation along the delay axis [Fig. 2(b)]. Frequency components of 1.0 eV (4.1 fs) are found at four photon energies: 56.9 eV, 58.0 eV, 58.3 eV, and 59.3 eV. The
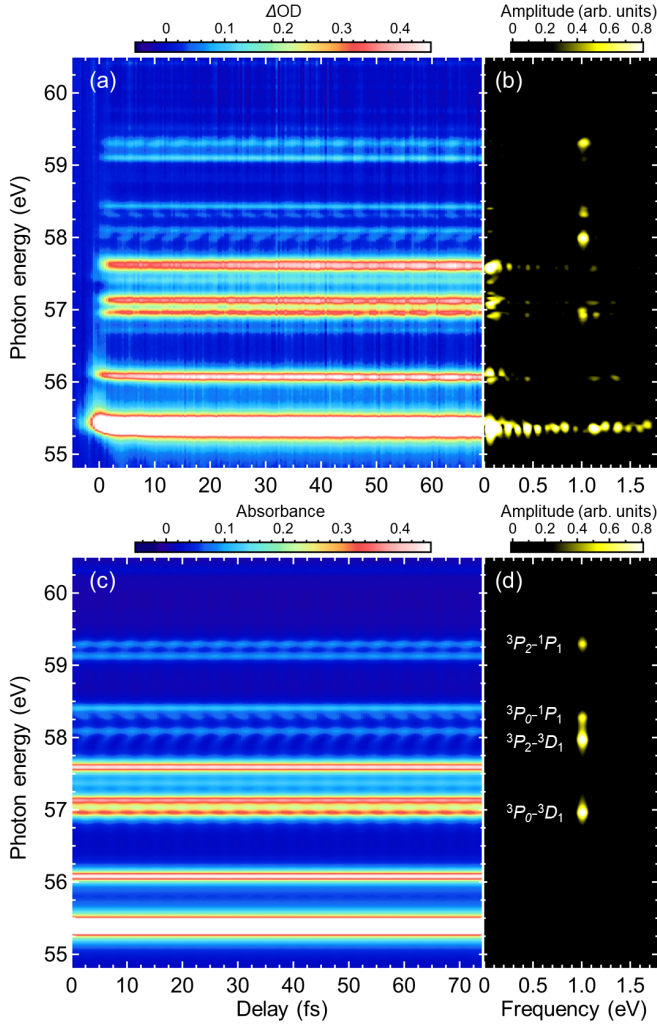
FIG. 2. (a) Experimental delay-dependent transient absorption spectra. The duration and the peak field intensity of the NIR pump pulse are 3.5 fs and 7×10^{14} W/cm^2. (b) Fourier transformation of the experimental results. Quantum beat signals with 1.0 eV frequency are seen at 56.9 eV, 58.0 eV, 58.3 eV, and 59.3 eV. (c) Simulated absorption spectra. The coherence is set between $^3P_2^0$-$^3P_0^0$ at $g = 0.4$. (d) Fourier transformation of the simulated results. The experimental signals at 1.0 eV are well reproduced, and their assignments are given.

observed quantum beats can be attributed to coherences from pairs of states with 1.0 eV energy separation; i.e., either $^3P_2$-$^3P_0$, or $^3P_1$-$^1D_2$, or both [Fig. 1(d)].

For assignments of the electronic states and coherences, a density matrix-based method is employed to simulate delay-dependent absorption spectra [34]. The method was originally developed for the $(4p)^{-1}$ configuration of Kr$^+$, and here it is extended to include generalized $(5p)^{-n}$ configurations of Xe^{n+} ($n = 1, 2, 3$) [26]. Briefly, the electronic states are expressed in a density matrix, and the core-to-valence absorption signals are treated analytically, assuming the probing XUV pulse is a delta function. The diagonal elements of the density matrix are characterized

by least-squares fitting to the static absorption spectrum [26]. States determined to have significant populations in Xe^{2+} are $^3P_2$, $^3P_0$, and $^3P_1$. No absorption signals originating from the higher-lying $^1D_2$ and $^1S_0$ states are observed [Fig. 1(c)]. Accordingly, the discussion hereafter focuses on those three states in the ^3P_J manifold.

Consideration of symmetry properties of the ion density matrix helps in limiting possible coherence pairs. It was shown that the density matrix possesses the following property [16]: $\rho_{J,J'}^{(-m)} = (-1)^{J-J'}\rho_{J,J'}^{(m)}$. For a matrix block with $m = 0$, the off-diagonal matrix elements are zero when $\Delta J = J - J'$ is odd. Note that this result is unique to Xe^{2+} where m is an integer, and it is a generalization of a previous finding explained as the cancellation of ionization pathways [20]. Application of the rules to the ^3P_J manifold leads to the conclusion that coherence can be produced only in two pairs of states, $^3P_2^0$-$^3P_0^0$ and $^3P_2^1$-$^3P_1^1$.

The simulated delay-dependent transient absorption spectra are shown in Fig. 2(c). In the simulation, coherence is taken to be between $^3P_2^0$-$^3P_0^0$ of Xe^{2+} at $g = 0.4$. It is found that the single coherence reproduces the experimentally observed quantum beats, and the corresponding core-to-valence transitions are identified to be from the $^3P_2$ and $^3P_0$ states of the valence configuration to the $^1P_1$ and $^3D_1$ states of the core-excited configuration. The degrees of coherence between two other pairs of states, $^3P_2^1$-$^3P_1^1$ of Xe^{2+} and $^2P_{3/2}^{1/2}$-$^2P_{1/2}^{1/2}$ of Xe$^+$, are evaluated by comparing the experimental signal-to-noise ratio and the simulated coherence signals, and they are both found to be less than the detection limits of the current experiments, $g < 0.09$ and $g < 0.02$, respectively [26].

Ionization time delays are extracted from the measured delay-dependent spectra. In the present transient absorption measurements, average ionization timings are defined as the center of the rise of the transient absorption signals, and the delays and standard deviations are determined by the least-squares fitting with error functions to the experimental spectral lines. The computed absorption signals from the states in the ^3P_J manifold are plotted in Figs. 3(a)–3(c) together with the experimental static transient absorption spectrum. The absorption signals at 57.1 eV, 57.0 eV, and 56.6 eV are associated one-to-one with the $^3P_2$, $^3P_0$, and $^3P_1$ states, respectively, and they are used to determine the time delay for each state. The signal from $^2P_{3/2}$ of Xe$^+$ at 55.4 eV is taken as a reference for the first ionization. The delays and one standard deviation determined for $^3P_2$, $^3P_0$, and $^3P_1$ are 0.85 ± 0.05 fs, 0.64 ± 0.07 fs, and 0.75 ± 0.05 fs, respectively [Figs. 3(d)–3(f)]. The delays are all shorter than half the optical cycle (1.3 fs), indicating a major contribution of double ionization within one laser half-cycle [35]. This result contrasts with a delay measured between Kr$^+$ and Kr^{2+}, 1.19 ± 0.20 fs, which is almost equal to one half of a laser cycle [36].
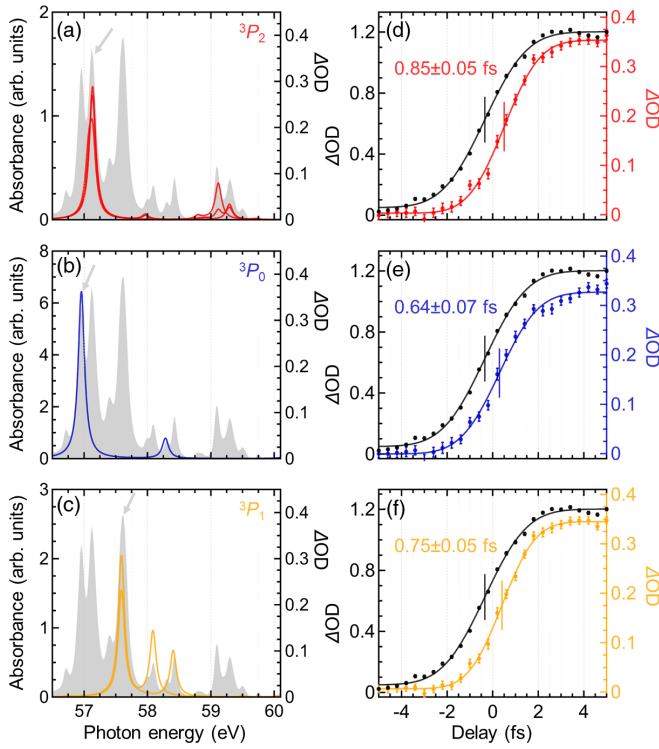
FIG. 3. (a)–(c) Core-to-valence absorption spectra computed for each state in the ^3P_J manifold (solid curves), plotted together with the experimental static transient absorption spectrum (gray area). The m-sublevels of $^3P_2$ and $^3P_1$ are overlaid in the same graph. The gray arrows indicate the absorption peaks that are used to determine the time delay. (d)–(f) Lineouts of the experimental transient absorption signals (dots with error bars) and the error-function fittings (solid curves). The signal from the $^3P_{3/2}$ state of Xe^+ at 55.4 eV is shown in black, and the signals from each state in the ^3P_J manifold are shown with colors. The vertical bars in the curves indicate the center of the rise.

The experimental results are compared with numerical simulations based on an uncorrelated electron-emission model [14]. Briefly, the ionic states are expressed in a density matrix. The action of the strong laser field is incorporated through the static ionization rate by ADK theory. The two ionization steps are treated independently, assuming there is no correlation between the released electrons. An empirical correction factor for the over-the-barrier ionization is added to the rate equations [37].

The calculated electronic coherences are shown in Fig. 4(a). The highest degree of coherence, $g = 0.44$, is predicted between the states $^3P_2^0$-$^3P_0^0$ of Xe^{2+}. Comparable degrees of coherence, $g = 0.29$ and $g = 0.21$, are also predicted between the states $^3P_2^1$-$^3P_1^1$ of Xe^{2+} and $^2P_{3/2}^{1/2}$-$^2P_{1/2}^{1/2}$ of Xe^+, respectively. Coherence is forbidden between $^3P_2^0$-$^3P_1^0$ and $^3P_0^0$-$^3P_1^0$, a result consistent with the aforementioned symmetry properties. Although the overall results are reasonable, the predicted coherences between $^3P_2^1$-$^3P_1^1$ and $^2P_{3/2}^{1/2}$-$^2P_{1/2}^{1/2}$ would be above the detection limits
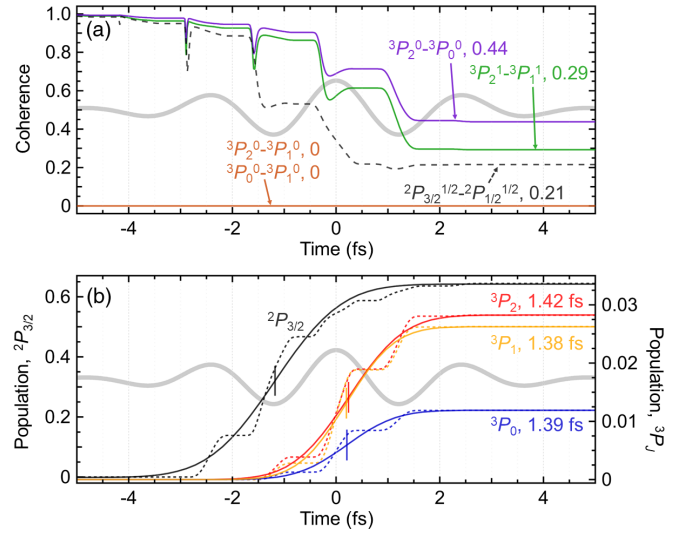

FIG. 4. (a) Simulated electronic coherences among the ^3P_J and ^2P_J manifolds with the experimental pump-pulse parameters. The gray curve shows the electric field of the pump pulse. The coherences g after the ionization are denoted next to the state labels. (b) Simulated electronic populations and ionization time delays. The dotted curves represent the simulated evolution of populations, and solid curves represent fitting results with error functions that are used to extract the rise times. The vertical bars in the curves indicate the center of the rise. The ionization time delays are denoted next to the state labels.

of the experiments. This inconsistency suggests that the selective coherence preparation mechanisms of strong-field double ionization are caused by the effects that are not included in the uncorrelated electron-emission model.

The ionization time delays in the simulations are determined based on the rise time of the populations [Fig. 4(b)]. The delays for $^3P_2$, $^3P_0$, and $^3P_1$ are 1.42 fs, 1.39 fs, and 1.38 fs, respectively. These delays are approximately equal to half of the optical cycle of the pump pulse, indicating a major contribution of ionization over two consecutive laser half-cycles. In addition, the simulations exhibit a weaker state dependence compared to what is detected by the experiments. Unexpectedly short delays have been observed in attoclock experiments for strong-field double ionization [20], and later theoretical studies have shown that the cause is attributed to electron correlation [21]. The observed short time delays are compatible with the results of the attoclock studies, and the state dependence of the delays among the ^3P_J manifold might be due to different degrees of contribution from electron correlation. Both the observed selectivity in coherence and the subfemtosecond time delays of specific states, neither of which is predicted by the uncorrelated electron-emission model, are suggestive of the role of electron correlation in strong-field double ionization. Investigation into how electron correlation might alter the formation of electronic coherences is an important topic requiring further theoretical analysis.

There are a few other possibilities missing from the uncorrelated electron-emission model. The most apparent is electron recollision-induced ionization, or nonsequential double ionization (NSDI) [38,39]. Previous intensity-dependent ion-yield measurements indicate that the present experimental field intensity (7×10^{14} W/cm^2) is well into the sequential ionization regime for xenon [40]. An experimental comparison of the transient absorption spectra taken separately with linearly and circularly polarized NIR fields shows only a $\sim 50\%$ reduction in the Xe^{2+} signals [26], which can be attributed just to the lower peak field intensity of the circularly polarized field. These observations indicate that sequential double ionization is a dominant process over NSDI in the present experiments. Another possibility is Stark shifts. On the grounds that the NIR laser field does not directly couple the valence $5p$ electrons to each other, Stark shifts are expected to be weak. In a previous theoretical study, Stark shifts in Xe$^+$ have been evaluated to be negligible even at the saturation field intensity for Xe$^+$ production [41], and thus effects from Stark shifts are presently considered unimportant to the observed coherences.

In summary, we have experimentally investigated coherent electron dynamics in xenon initiated by strong-field double ionization. The all-optical transient absorption method employed here provides a successful strategy for the simultaneous characterization of electronic coherences and ionization timings in multiple electronic states. Selective preparation of electronic coherence has the potential to steer charge migration and accompanying bond rearrangement processes, a possibility that connects to the concept known as charge-directed reactivity [42]. We anticipate that the present study will provide an experimental benchmark for theoretical models to explain the unexplored roles of electron correlation in strong-field ionization dynamics.

---

[*]ykoba@berkeley.edu
[†]dneumark@berkeley.edu
[‡]srl@berkeley.edu

[1] F. Krausz and M. Ivanov, Rev. Mod. Phys. 81, 163 (2009).
[2] K. Ramasesha, S. R. Leone, and D. M. Neumark, Annu. Rev. Phys. Chem. 67, 41 (2016).
[3] Z. Chang, P. B. Corkum, and S. R. Leone, J. Opt. Soc. Am. B 33, 1081 (2016).
[4] E. Goulielmakis, Z.-H. Loh, A. Wirth, R. Santra, N. Rohringer, V. S. Yakovlev, S. Zherebtsov, T. Pfeifer, A. M. Azzeer, M. F. Kling, S. R. Leone, and F. Krausz, Nature (London) 466, 739 (2010).
[5] A. Wirth, M. T. Hassan, I. Grguraš, J. Gagnon, A. Moulet, T. T. Luu, S. Pabst, R. Santra, Z. A. Alahmed, A. M. Azzeer, V. S. Yakovlev, V. Pervak, F. Krausz, and E. Goulielmakis, Science 334, 195 (2011).
[6] C. Ott, A. Kaldun, L. Argenti, P. Raith, K. Meyer, M. Laux, Y. Zhang, A. Blättermann, S. Hagstotz, T. Ding, R. Heck, J. Madroñero, F. Martín, and T. Pfeifer, Nature (London) 516, 374 (2014).
[7] P. M. Kraus, B. Mignolet, D. Baykusheva, A. Rupenyan, L. Horný, E. F. Penka, G. Grassi, O. I. Tolstikhin, J. Schneider, F. Jensen, L. B. Madsen, A. D. Bandrauk, F. Remacle, and H. J. Wörner, Science 350, 790 (2015).
[8] A. Fleischer, H. J. Wörner, L. Arissian, L. R. Liu, M. Meckel, A. Rippert, R. Dörner, D. M. Villeneuve, P. B. Corkum, and A. Staudte, Phys. Rev. Lett. 107, 113003 (2011).
[9] F. Calegari, D. Ayuso, A. Trabattoni, L. Belshaw, S. De Camillis, S. Anumula, F. Frassetto, L. Poletto, A. Palacios, P. Decleva, J. B. Greenwood, F. Martín, and M. Nisoli, Science 346, 336 (2014).
[10] D. M. Villeneuve, P. Hockett, M. J. J. Vrakking, and H. Niikura, Science 356, 1150 (2017).
[11] F. Lépine, M. Y. Ivanov, and M. J. J. Vrakking, Nat. Photonics 8, 195 (2014).
[12] T. Brabec and F. Krausz, Rev. Mod. Phys. 72, 545 (2000).
[13] M. V. Ammosov, N. B. Delone, and V. P. Krainov, Sov. Phys. JETP 64, 1191 (1986).
[14] A. N. Pfeiffer, S. G. Sayres, and S. R. Leone, Mol. Phy. 111, 2283 (2013).
[15] S. Pabst, M. Lein, and H. J. Wörner, Phys. Rev. A 93, 023412 (2016).
[16] N. Rohringer and R. Santra, Phys. Rev. A 79, 053402 (2009).
[17] I. V. Litvinyuk, F. Légaré, P. W. Dooley, D. M. Villeneuve, P. B. Corkum, J. Zanghellini, A. Pegarkov, C. Fabian, and T. Brabec, Phys. Rev. Lett. 94, 033003 (2005).
[18] T. Åberg, Phys. Rev. A 2, 1726 (1970).
[19] T. Y. Shi and C. D. Lin, Phys. Rev. Lett. 89, 163202 (2002).
[20] A. N. Pfeiffer, C. Cirelli, M. Smolarski, R. Dörner, and U. Keller, Nat. Phys. 7, 428 (2011).
[21] Y. Zhou, C. Huang, Q. Liao, and P. Lu, Phys. Rev. Lett. 109, 053004 (2012).
[22] A. Wirth, R. Santra, and E. Goulielmakis, Chem. Phys. 414, 149 (2013).
[23] In the term symbol notation, S, L, and J represent the spin quantum number, orbital quantum number, and total angular momentum, respectively. The quantum number m represents the projection of the total angular momentum along the laser polarization axis, and this is omitted when only the energy is relevant.
[24] H. Timmers, Y. Kobayashi, K. F. Chang, M. Reduzzi, D. M. Neumark, and S. R. Leone, Opt. Lett. 42, 811 (2017).
[25] M. Miranda, T. Fordell, C. Arnold, A. L'Huillier, and H. Crespo, Opt. Express 20, 688 (2012).
[26] See Supplemental Material at http://link.aps.org/supplemental/10.1103/PhysRevLett.120.233201 for details of the analysis on coherence, the comparison between linearly and circularly polarized measurements, the method to estimate the xenon gas pressure, and the results of additional measurements at different xenon pressures. Supplemental Material includes Refs. [27,28].
[27] H. Kaiser, Anal. Chem. 42, 26A (1970).

[28] D. L. Ederer and M. Manalis, J. Opt. Soc. Am. **65,** 634 (1975).

[29] S. G. Sayres, E. R. Hosler, and S. R. Leone, J. Phys. Chem. A **118,** 8614 (2014).

[30] M. Sabbar, H. Timmers, Y.-J. Chen, A. K. Pymer, Z.-H. Loh, S. G. Sayers, S. Pabst, R. Santra, and S. R. Leone, Nat. Phys. **13,** 472 (2017).

[31] Y. Kobayashi, H. Timmers, M. Sabbar, S. R. Leone, and D. M. Neumark, Phys. Rev. A **95,** 031401 (2017).

[32] M. Sabbar, S. Heuser, R. Boge, M. Lucchini, L. Gallmann, C. Cirelli, and U. Keller, Rev. Sci. Instrum. **85,** 103113 (2014).

[33] R. D. Cowan, *The Theory of Atomic Structure and Spectra* (University of California Press, Berkeley, 1981).

[34] R. Santra, V. S. Yakovlev, T. Pfeifer, and Z.-H. Loh, Phys. Rev. A **83,** 033405 (2011).

[35] M. S. Schöffler, X. Xie, P. Wustelt, M. Möller, S. Roither, D. Kartashov, A. M. Sayler, A. Baltuska, G. G. Paulus, and M. Kitzler, Phys. Rev. A **93,** 063421 (2016).

[36] A. Wirth, Attosecond transient absorption spectroscopy, Ph. D. thesis, Ludwig-Maximilian-Universität München, 2011.

[37] X. M. Tong and C. D. Lin, J. Phys. B **38,** 2593 (2005).

[38] P. B. Corkum, Phys. Rev. Lett. **71,** 1994 (1993).

[39] B. Walker, B. Sheehy, L. F. DiMauro, P. Agostini, K. J. Schafer, and K. C. Kulander, Phys. Rev. Lett. **73,** 1227 (1994).

[40] S. Larochelle, A. Talebpour, and S. L. Chin, J. Phys. B **31,** 1201 (1998).

[41] R. Santra, R. W. Dunford, and L. Young, Phys. Rev. A **74,** 043403 (2006).

[42] F. Remacle and R. D. Levine, Proc. Natl. Acad. Sci. U.S.A. **103,** 6793 (2006).